第 30 卷第 10 期
2014 年 10 月

无 机 化 学 学 报
CHINESE JOURNAL OF INORGANIC CHEMISTRY

Vol.30 No.10
2453-2460

盐酸刻蚀的不同形貌空心结构二氧化锰的电化学行为

韩丹丹 徐鹏程* 丁元生 朱长凤 柏铭阳 刘乙良
(吉林化工学院化学与制药工程学院,吉林 132022)

摘要: 以液相湿法和水热法合成的碳酸锰为前驱体,通过盐酸的选择性刻蚀分别合成立方体和纺锤体 MnO_2 分级空心结构。采用 X 射线衍射(XRD)、扫描电镜(SEM)和透射电子显微镜(TEM)对其结构和形貌进行了表征。采用循环伏安、恒流充放电技术和交流阻抗对其电化学性能进行了测试。结果表明,碳酸锰前驱体粒径分布集中,简易快速(3 min)的合成技术所形成的空心结构有利于电解液的渗透,以及电子和离子的传输与交换。在电流密度为 0.5 A·g^{-1} 时,分级空心立方体 MnO_2 电极比电容为 115 F·g^{-1},并表现出良好的循环稳定性和可逆性。

关键词: MnO_2; 盐酸刻蚀; 微纳米空心结构;电 化学性能
中图分类号: O646 **文献标识码**: A **文章编号**: 1001-4861(2014)10-2453-08
DOI:10.11862/CJIC.2014.316

Capacitance Behavior of Manganese Oxide Hollow Structures with Different Morphologies via Hydrochloric Acid Chemical Etching

HAN Dan-Dan XU Peng-Cheng* DING Yuan-Sheng ZHU Chang-Feng BAI Ming-Yang LIU Yi-Liang
(*College of Chemistry and Pharmaceutical Engineering, Jilin Institute of Chemical Technology, Jilin, Jilin* 132022, *China*)

Abstract: Hierarchical hollow MnO_2 were controllably synthesized by hydrochloric acid chemical etching. $MnCO_3$ with spindle and cube morphology was used as the precursor. The microstructure and morphologies of the resulting materials were characterized by XRD, SEM, TEM and electrochemical measurements. The results indicate that the product obtained by simple reaction for 3 min has hollow structure with excellent permeability, narrow pore-size distribution, and favorable capacitance performance. Further, due to facile mass transfer in the perfectly porous matrix, the synthesized MnO_2 show lower equivalent series resistance and better frequency response as revealed from the impedance studies.

Key words: manganese oxide; hydrochloric acid chemical etching; micro-nano hollow structure; electrochemical performance

Supercapacitors, a characteristic combination of high power and reasonable energy density with faster response time and near-infinite life cycle in a wide operational temperature range, can complement other energy storage devices like conventional capacitors, batteries and fuel cells. However, in some new application fields, such as electric and hybrid vehicles, supercapacitor with higher capacitance and longer cycle life is necessary[1-5].

MnO_2 appears to be one of the most attractive electrode materials for supercapacitors, due to its low cost, availability, environmental friendliness, and higher capacitance[6-9]. However, the supercapacitive performance of a MnO_2 electrode depends on the

收稿日期:2014-05-06。收修改稿日期:2014-06-30。
国家自然科学基金(No.201401073),吉林省科技厅青年基金(No.20140520097JH)、吉林省教育厅“十二五”科技项目(No.2012290)、博士科研启动基金(No.2014161)、吉林化工学院科技项目(No.2013053、2014064)资助项目。
*通讯联系人。E-mail:luckhan2006@163.com

particle size of the active material, electrode morphology, and its crystal structure. In addition, the hollow structured active material for the supercapacitor electrode is a critical issue in overcoming the intrinsically low electronic conductivity and clustered morphology of MnO_2[10-11]. A literature survey show that many routes or techniques for preparation of MnO_2 have been developed, such as sonochemical synthesis[12], solution-combustion[13], thermal decomposition[14], hydrothermal synthesis[10,15], microwave-assisted synthesis[16-17] electro-deposition[18] and sol-gel progress[7]. However, most of the methods require extensive mechanical mixing, long duration, high temperature, high energy-consuming, which are employed to generate bulk nanostructures and films of MnO_2 for supercapacitor applications.

Herein, we report the synthesis of different MnO_2 hollow structures, such as cubes and spindles. The method developed here is based on etching the $MnCO_3$ template by hydrochloric acid, the morphologies of which can be easily controlled by varying the morphologies of the $MnCO_3$ intermediate. The crystal structure of MnO_2 was investigated to elucidate the formation mechanism of the products. The electrochemical properties of these hollow structures were also evaluated.

1 Experimental

1.1 Synthesis procedure

All the chemicals were of analytical grade and were used without further purification. $MnCO_3$ microcubes were prepared base on Qian′s group method[19] with minor modification. Briefly, 0.2 g of $MnSO_4$, 1 g of $NaHCO_3$, and 1.5 g of $(NH_4)_2SO_4$ were added to a given amount of distilled water and 7 mL ethanol, maintaining for 8 h in an oven at 50 ℃.

$MnCO_3$ spindles were prepared by dissolving 0.35 g of $MnCl_2$ into 28 mL of deionized water. Then 0.42 g of $Na_3C_6H_5O_7$ was added, and the resulting solution was stirred for 10 min to form a homogeneous mixture, and finally 2.1 mL of NH_3 (25%) was added to the above solution. The mixture was then transferred into a 50 mL Teflon-lined (PTFE) stainless steel autoclave. The autoclave was sealed and kept in an oven at 160 ℃ for 2 h.

The as-prepared $MnCO_3$ sample was dispersed in 20 mL of distilled water, and then 0.03 mol·L^{-1} $KMnO_4$ solution was added under stirring. After 2 min, 2.5 mol·L^{-1} hydrochloric acid was added into the above solution, and the mixturewas maintained at room temperature with stirring for 1 min. Finally, the hollow MnO_2 was separated, and washed with double distilled water several times, and dried in a vacuum at 60 ℃ for 12 h. The hollow spindle- and cube-MnO_2 structures with were denoted as MnO_2-s and MnO_2-c, respectively.

1.2 Characterization

XRD patterns were recorded on a Rigaku D/max TTR-III diffractometer using Cu $K\alpha$ radiation (λ = 0.154 18 nm). The morphologies of the sample were observed on a scanning electron microscope (SEM, JSM-6480A, Japan Electronics). TEM micrographs were taken on a FEI Tecnai G^2 20 S-TWIN transmission electron microscope with a field emission gun operating at 200 kV.

1.3 Preparation of electrodes and electrochemical characterization

To evaluate the electrochemical properties of the MnO_2 microstructures, working electrodes were prepared as follows. The as-prepared materials, graphite, acetylene black, and poly (tetrafluoroethylene) (PTFE) were mixed in a mass ratio of 75∶10∶10∶5 and dispersed in ethanol to produce a homogeneous paste. Graphite, acetylene black and PTFE were used as the conductive agent and binder, respectively. Then the mixture was coated onto the nickel foam substrate (1 cm^2) with a spatula. Finally, the fabricated electrodes were dried at 60 ℃ for 1 d in a vacuum oven. The loading level of the active material on the current collector is typically 0.02 g·cm^{-2}. Cyclic voltammetry (CV), chronopotentiometry (CP), and electrochemical impedance spectroscopy (EIS) measurements were carried out using conventional three-electrode configuration on a CHI 660 E electrochemical workstation. The Ni foam coated with MnO_2 was used as the working electrode, and platinum foil (1 cm^2) and a

saturated calomel electrode (SCE) were used as the counter and reference electrode. All the experiments were carried out using freshly prepared 1.0 mol·L^{-1} aqueous $NaSO_4$ electrolyte. The EIS measurements were carried out in the frequency range from 100 kHz to 0.05 Hz at open circuit potential with an ac perturbation of 5 mV.

2 Results and discussion

2.1 Material characterization

The XRD results of (a) hierarchical hollow cubes, (b) hollow spindles MnO_2 and (c) $MnCO_3$ cubes precursors are given in Fig.1. All of the diffractions of the XRD pattern in Fig.1c can be readily indexed to pure hexagonal phase of $MnCO_3$ according to reported data (PDF No.86-0173). The narrow and strong peaks in the XRD pattern are mainly attributed to the high crystallinity. As shown in Fig.1a, the pattern of the as-prepared sample matches well with the standard pattern of the hexagonal ε-MnO_2 (PDF No.30-0820, a =0.280 nm, c=0.445 nm). No peaks for other types of MnO_2 are observed, indicating that the ε-MnO_2 have been successfully prepared from the pure phase hexagonal $MnCO_3$, whereas for pattern b, apart from the peaks of the rhombohedral $MnCO_3$, some peaks

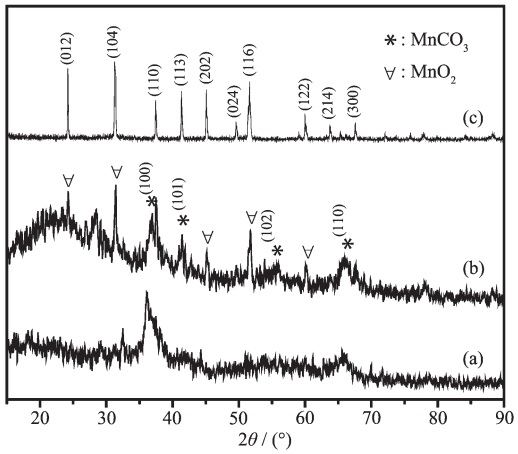

Fig.1 XRD patterns of the as-prepared ε-MnO_2 (a) hierarchical hollow spindles, (b) hollow cubes and (c) $MnCO_3$ precursor

that originate from the $MnCO_3$ intermediate are also found.

The SEM images of spindle $MnCO_3$ precursor with different magnifications are shown in Fig.2a,b. It is clear from Fig.2a that the sample exhibits a uniform and spindle-like structure with a length of several micrometers. Fig.2b (high magnification) clearly shows sphere-like structure with length of 2 μm, which may be formed by the rupture from the thinnest of the spindles during the hydrothermal process. However, the growth of spindles with a rough surface is evident.

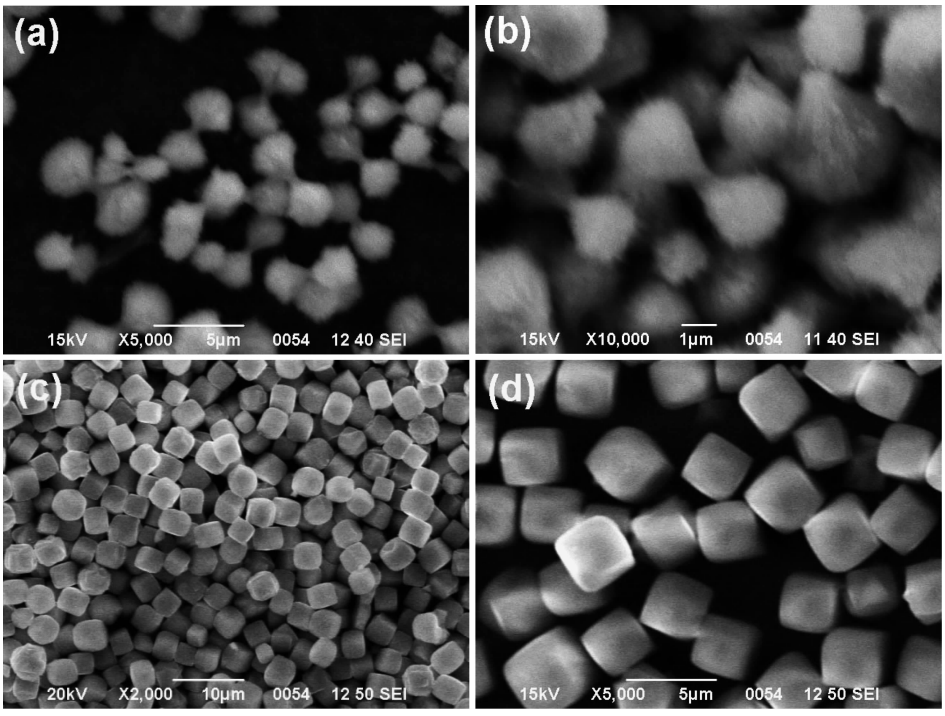

Fig.2 SEM images for different shaped $MnCO_3$ structures: (a, b) spindles and (c, d) cubes

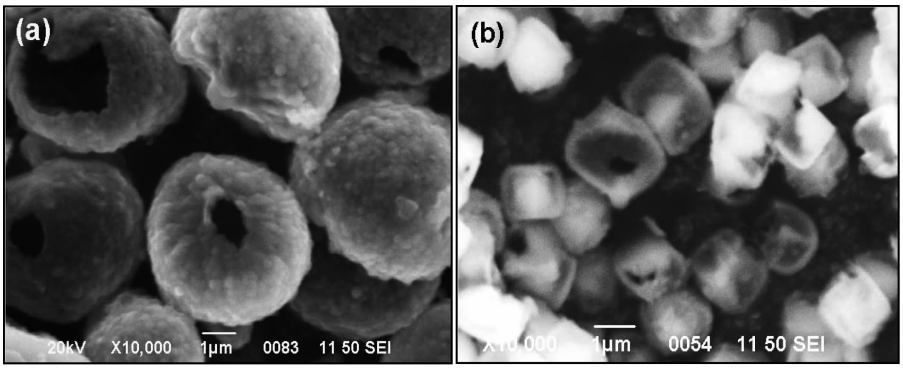

Fig.3 SEM images for different shaped hollow MnO_2 structures: (a) spindles and (b) cubes

As shown in Fig.2c,d the microcubes exhibit the average edge length of 2.5~3 μm. The hollow MnO_2 with hierarchical structure is obtained by the oxidation of the spherical precursor crystals in $KMnO_4$ solution at room temperature followed by removal of $MnCO_3$ with HCl. Fig.3a and b show the SEM images of MnO_2 hollow structure. One can see that the as-obtained MnO_2 maintains the frame structure of the precursor. At a high magnification (Fig.2b), there is a mouth-like opening on some of the cubes and spindles. Through the opening, the inner hollow structure can be clearly seen.

The low-magnification TEM images in Fig.4a and c show cube-and spindle-MnO_2 with clearly visible hollow interiors. As shown, numerous nanoparticles are with irregular aggregation and form hierarchical shell of spindle-MnO_2 structures (Fig.4b). Fig.4d confirms the hollow MnO_2 microcubes structure with a wall thickness of 100~200 nm. The SEM and TEM analysis reveal that this unique open mesoporous morphological characteristic is favorable for electrolyte penetration and fast ion/electron transfer and may lead to increasing of the electrochemical reactivity.

The synthetic mechanism of $KMnO_4$ with $MnCO_3$

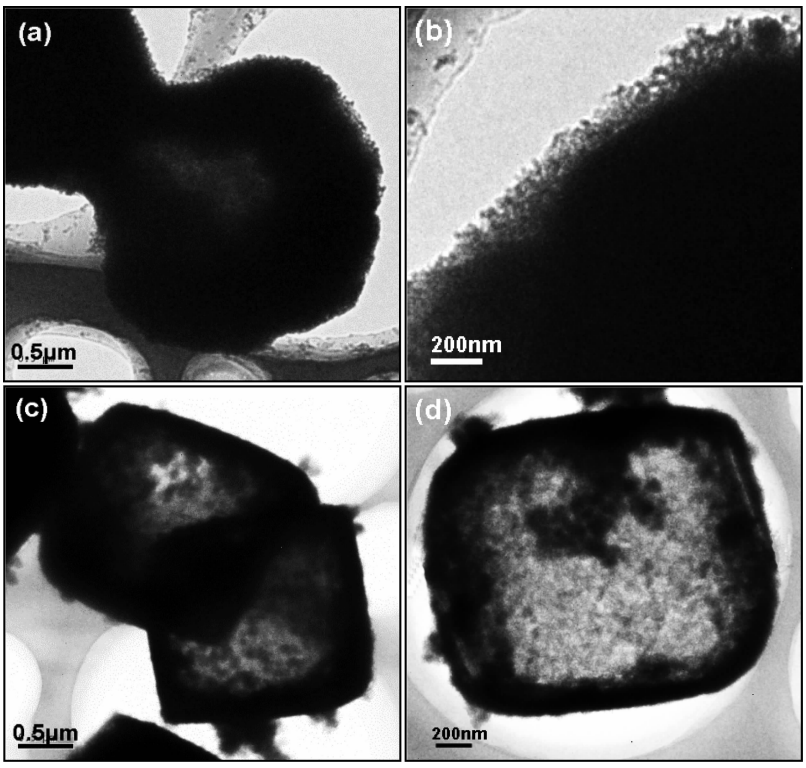

Fig.4 TEM images for different shaped hollow MnO_2 structures: (a) overview of spindles, (b) cubes, (c) edge of a spindles MnO_2 shell and (d) a single cubes

around the micrometersized precursor surface could be explained by a Kirkendall effect[20-21], as shown in Fig.5. The MnO_2 shell with $MnCO_3$ intermediate core is prepared at room temperature using a freshly prepared solution of dilute $KMnO_4$ to oxidize the surface of the $MnCO_3$ intermediate. $KMnO_4$ and $MnCO_3$ can react with each other readily and form a diffusion pair. The coupled reaction/diffusion at the crystal/solution interface might lead to the quick formation of a MnO_2 shell around the outside surfaces of the $MnCO_3$ crystals. After removal of the $MnCO_3$ intermediate core with HCl, well crystallized MnO_2 hierarchical hollow structure was obtained. There has always been a strong correlation between the crystallinity structure and the surface area of the system on the electrochemical properties as discussed later.

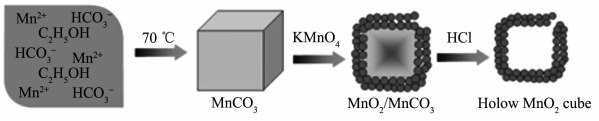

2.2 Electrochemical characterizations

The CV responses of the MnO_2-s and MnO_2-c sample at different scan rates (10~50 mV·s^{-1})in a fixed potential range of −0.2~0.8 V in aqueous 1 mol·L^{-1} Na_2SO_4 electrolyte are shown in Fig.6a and Fig.6c, respectively. The individual MnO_2-s and MnO_2-c sample electrodes are subjected to one time stabilization/activation by repeated CV cycles (25 numbers) at sweep rate of 50 mV·s^{-1} in the similar potential range, before performing the CV experiments for accessing the electrochemical performance. The CV profiles of MnO_2 sample at different scan rates are almost rectangular in shape indicative of ideal pseudocapacitive behavior. In neutral electrolyte as studied here, there are generally two parallel mechanisms proposed, based on the adsorption and intercalation involving surface and bulk phenomena during the charge storage in porous MnO_2-based

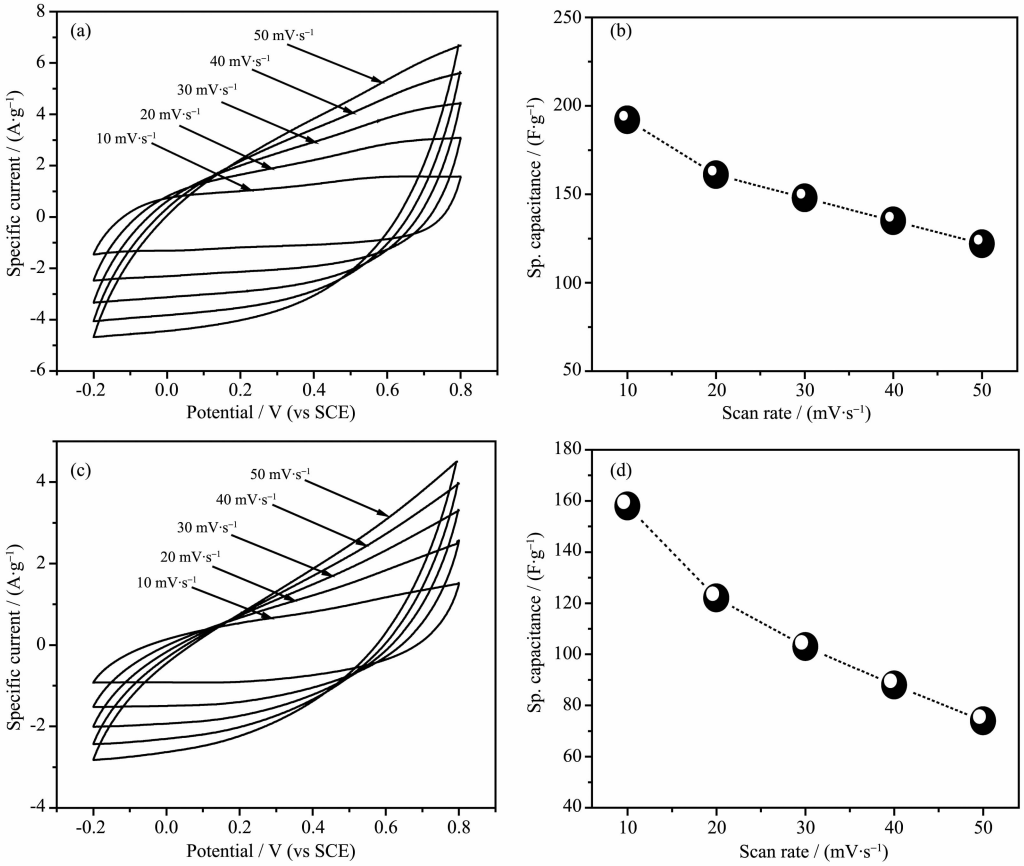

Fig.6 (a, c) Cyclic voltammetry curves of hierarchical hollow MnO_2-c and MnO_2-s samples at scan rate of 10, 20, 30, 40 and 50 mV·s^{-1}; (b, d) specific capacitance as a function of scan rate with different structure

electrodes[22-24]. The first possible mechanism is ascribed to the rapid intercalation of alkali metal cations such as Na^+ in the electrode during reduction and deintercalation upon oxidation.

$$MnO_2+C^++e^- \rightleftharpoons MnOO^-C^+$$

The other possible mechanism is based on the adsorption of the H^+ and Na^+ ions on the surface, rather than in the bulk of the sample[22,25-27].

$$MnO_{2(surface)}+C^++e^- \rightleftharpoons (MnO_2^-C^+)_{(surface)}$$

where C can be either H^+ or Na^+ ion. This clearly demonstrates the occurrence of intercalation and deintercalation of H^+ or Na^+ ions during the charge storage in the MnO_2 sample. This is due to the fact that at lower scan rates, both outer- and the inner-pore surfaces of the porous electrode materials are effectively utilized for intercalation, while at high scan rates mainly outer regions of the pores are accessed by the ions. However, the cathodic and the anodic peak currents of MnO_2-c sample are slightly higher than MnO_2-s sample, implying a higher specific capacitance. From the CV measurements at different scan rates (v, $mV\cdot s^{-1}$), the specific capacitance (C_s, $F\cdot g^{-1}$) values are estimated using the equation[28-29]:

$$C_s=\frac{1}{vw(V_a-V_c)}\int_{V_a}^{V_c} iV\mathrm{d}V \qquad (1)$$

where w (g) is active weight of the electrode material. The specific capacitance values of the sample at different scan rates are drawn from the integration of potential (V versus SCE) versus specific capacitance (C_s, $F\cdot g^{-1}$) graphs, as shown in Fig.6b,c. At potential scan rates of 10~50 $mV\cdot s^{-1}$, the specific capacitance values for MnO_2-c sample are 189~112 $F\cdot g^{-1}$. Similarly, at the same scan rate the specific capacitance values for MnO_2-s sample are in the range of 158~74 $F\cdot g^{-1}$. As the scan rate increases, the specific capacitance values decrease, which is due to the limitation of the ion diffusion rate to satisfy electronic neutralization during the charge and discharge reaction.

The rate dependent discharge profiles taken from the first cycle of corresponding voltage time profiles of MnO_2-c and MnO_2-s samples are shown in Fig.7a and b, respectively. It is noted that the discharging time of MnO_2-c sample is higher than that of MnO_2-s sample at identical current density conditions. The specific capacitance of the electrode is obtained from the following equation[30-33]:

$$C=\frac{I}{[(\mathrm{d}V/\mathrm{d}t)w]} \qquad (2)$$

where I (A) and $\mathrm{d}V/\mathrm{d}t$ ($V\cdot s^{-1}$), respectively, denote the applied galvanostatic current and the slope of chronopentionmetric curve, w (g) represents the mass of electroactive material. It can be ascertained that the specific capacitance of MnO_2-c sample is 115 $F\cdot g^{-1}$ as compared to 90 $F\cdot g^{-1}$ by MnO_2-s sample at current density of 0.5 $A\cdot g^{-1}$. It indicates that the enhanced rate capability capacitance of MnO_2-c sample is a combined contribution of much thinner shell with superior pore channel and large internal accessible surface which in turn facilitates the electrolyte penetration into the sample matrix, decreases the ion

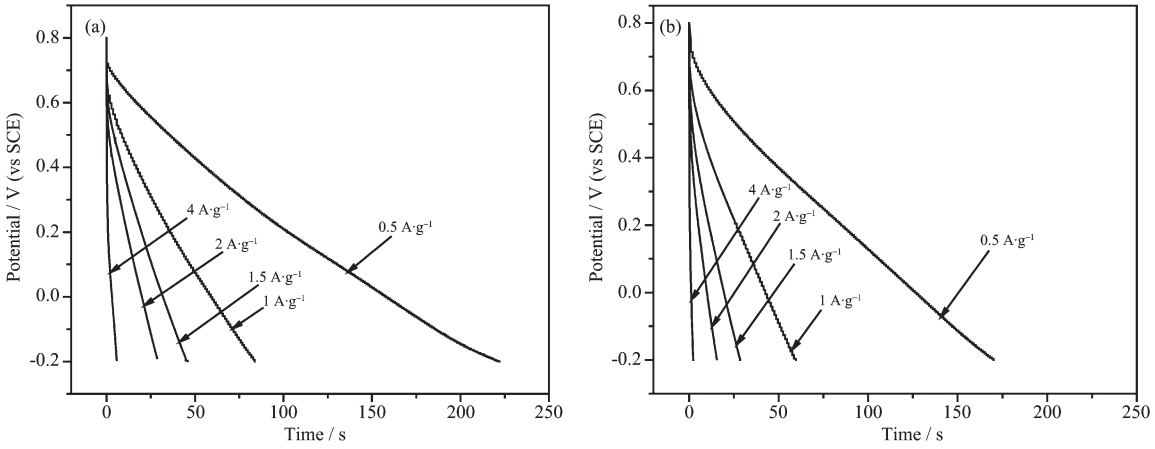

Fig.7 Discharge curves of (a) MnO_2-c sample and (b) MnO_2-s sample between voltage limits of –0.2 to 0.8 V at rates from 0.5 $A\cdot g^{-1}$ to 4$A\cdot g^{-1}$

diffusion resistance and enhances the electroactive surface utilization during the charge and discharge process[34].

The EIS has been employed to study the kinetic features of MnO_2-c sample electrodes during their charge storage process[35]. For both the samples, the complex-plane impedance plots fitted by complex nonlinear least squares (CNLS) fitting method to the Randle equivalent circuit are shown in Fig.8. where C_d in parallel with a charge-transfer resistor is a double layer capacitor, W is Warburg impedance, and R_{ict} is charge transfer resistance at the electrode electrolyte interface due to the discontinuity in the charge transfer process because of conductivity difference between the solid oxide (electronic conductivity) and liquid electrolyte phase (ionic conductivity). The distinctive semicircle of the MnO_2 sample after charge-discharge cycles in the medium frequency region is small as compared to that before the cycles, suggesting lower diffusion resistance during insertion/de-insertion of H^+ and Na^+ ions inside the matrix of porous MnO_2 sample. A major difference is the slope of the 45° portion of the curve called the Warburg resistance (Z_W), which is a result of the frequency dependence of ion diffusion/transport in the electrolyte to the electrode surface[36]. Moreover, the increased Warburg resistance after 500 cycles is attributed to the increased diffusion and migration pathways of electrolyte ions during the charge/discharge processes. Long cycling life is an important

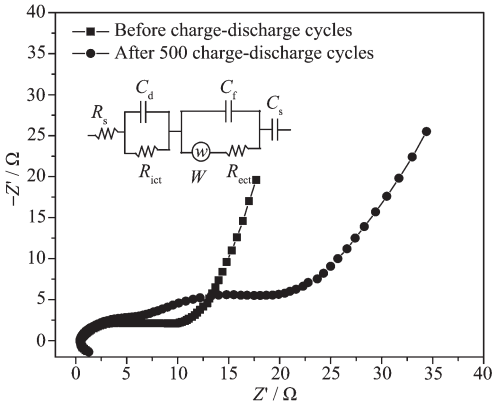

Fig.8　Nyquist plots of MnO_2-c electrode before and after 500 cycles; Inset shows the electrical equivalent circuit used for fitting impedance spectra

requirement for supercapacitors[37]. The cycling life test over 500 cycles for the MnO_2-c and MnO_2-s sample electrodes was carried out by repeating the galvanostatic charge-discharge test between −0.2 and 0.8 V at a current density of 0.5 A·g^{-1}. The capacitance retention of 83% is observed after 500 cycles, which is higher for MnO_2-c sample as compared to MnO_2-s sample. These results indicate that the hierarchical superstructure endow the hollow urchins with excellent rate capability and long cycling stability.

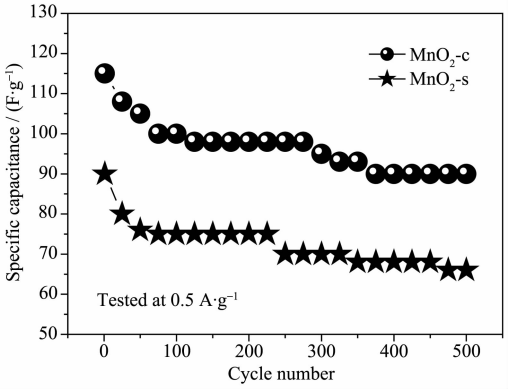

Fig.9　Specific discharge capacity of MnO_2-c and MnO_2-s sample tested for 500 cycles at a current density of 0.5A·g^{-1}

3　Conclusions

In summary, 3D hierarchical ε-MnO_2 microcubes and spindles have been prepared by shape-preserving $KMnO_4$ oxidation of micrometer-scale manganese carbonate structures. The formation of the unique superstructure stems from Kirkendall effect and chemical etching by hydrochloric acid. The electrochemical studies indicate the product shows a specific capacitance value of 115 F·g^{-1} with excellent rate capability and good cycling stability. Furthermore, the asprepared materials with distinct morphology may find potential applications in the fields of supercapacitors, catalysts, absorbents, sensors, electromagnetic and microelectronic devices.

References:

[1] Conway B E. *Electrochemical Supercapacitors*: *Scientific Fundamentals and Technological Applications*. New York:

Kluwer Academic/Plenum Publishers, , **1999**.
[2] Kötz R, Carlen M. *Electrochim. Acta*, **2000**,**45**:2483-2498
[3] Han D D, Jing X Y, Wang J, et al. *J. Electroanal. Chem.*, **2012**,**682**:37-44
[4] Simon P, Gogotsi Y *Nat. Mater.*, **2008**,**7**:845-854
[5] Hu L, Choi J W, Yang Y, et al. *Proc. Natl. Acad. Sci. U.S.A.*, **2009**,**106**:21490-21494
[6] Rios E C, Rosario A V, Mello R M. *J. Power Sources*, **2007**, **163**:1137-1142
[7] Lee H Y, Goodenough J B. *J. Solid State Chem.*, **1999**,**144**: 220-223
[8] Stankovich S, Dikin D A, Piner R D, et al. *Carbon*, **2007**,**45**: 1558-1565
[9] Wang Y G, Li H Q, Xia Y Y, et al. *J. Adv. Mater.*, **2006**,**19**: 2619-2623
[10]GUI Yi-Cai(桂义才), QIAN Li-Wu(钱立武), QIAN Xue-Feng(钱雪峰). *Chinese J. Inorg. Chem.*(无机化学学报), **2009**,**25**(4):668-673
[11]Gu Y, Cai J W, He M Z, et al. *J. Power Sources*, **2013**,**239**: 347-355
[12]Ghaemi M, Ataherian F, Zolfaghari A, et al. *Electrochim. Acta*, **2008**,**53**:4607-4930
[13]Hong X G, Xi Z L, Wen W. *Inorg. Chem. Commun.*, **2010**, **13**:909-913
[14]Beaudrouet E, Le Gal La Salle A, Guyomard D. *Electrochim. Acta*, **2009**,**54**:1240-1248
[15]Chen K F, Noh Y D, Li K Y, et al. *J. Phys. Chem. C*, **2013**, **117**:10770-10779
[16]Ming B S, Li J L, Kang F Y, et al. *J. Power Sources*, **2012**, **198**:428-431
[17]Meher S K, Rao G R. *J. Power Sources*, **2012**,**215**:317-328
[18]Jana S K, Rao V P, Banerjee S. *Chem. Phys. Lett.*, **2014**, **593**:160-164
[19]Cao J, Zhu Y C, Bao K Y, et al. *J. Phys. Chem. C*, **2009**, **113**:17755-17760
[20]Fei J B, Cui Y, Yan X H, et al. *Adv. Mater.*, **2008**,**20**:452-456
[21]Smigelskas A D, Kirkendall E O. *Trans. Am. Inst. Min. Metall. Pet. Eng.*, **1947**,**171**:130-136
[22]Minga B S, Li J L, Kang F Y, et al. *J. Power Sources*, **2012**, **198**:428-431
[23]XUE Zhao-Hui(薛兆辉), LIU Zhao-Lin(刘兆临), MA Fang-Wei(马方伟), et al. *Chinese J. Inorg. Chem.*(无机化学学报), **2000**,**16**(2):287-292
[24]Wan J G, Yang Y, Huang Z H, et al. *Electrochim. Acta*, **2014**,**130**:642-649
[25]Zhao Y, Meng Y N, Jiang P. *J. Power Sources*, **2014**,**259**: 219-226
[26]Xu C, Wei C, Li B, et al. *J. Power Sources*, **2011**,**196**:7854-7859
[27]Nayak P K, Munichandraiah N. *J. Electrochem. Soc.*, **2011**, **158**:A585-A591
[28]Han D D, Xu P C, Jing X Y, et al. *J. Power Sources*, **2013**, **235**:45-53
[29]Meher S K, Justin P, Ranga Rao G. *Electrochim. Acta*, **2010**,**55**:8388-8396
[30]Hu C C, Chang K H, Hsu T Y. *J. Electrochem. Soc.*, **2008**, **155**:F196-F200
[31]Stoller M D, Park S J, Zhu Y W, et al. *Nano Lett.*, **2008**,**10**: 3498-3502
[32]Xia X H, Chao D L, Qi X Y, et al. *Nano Lett.*, **2013**,**13**: 4562-4568
[33]Dubal D P, Gund G S, Lokhande C D, et al. *ACS Appl. Mater. Interfaces*, **2013**,**5**:2446-2454
[34]Byoungwoo K, Gerbrand C. *Nature*, **2009**,**458**:190-195
[35]Sugimoto W, Iwata H, Yokoshima K, et al. *J. Phys. Chem. B*, **2005**,**109**:7330-7338
[36]Hasan M, Jamal M, Razeeb K M. *Electrochimi. Acta*, **2012**, **60**:193-200
[37]Hou Y, Cheng Y W, Hobson T, et al. *Nano Lett.*, **2010**,**10**: 2727-2733